PROCEEDINGS OF SCIENCE

The hadronic running of the electromagnetic coupling and electroweak mixing angle

Teseo San José,[a,b,c,*] **Hartmut Wittig,**[a,b,c,*] **Marco Cè,**[d] **Antoine Gérardin,**[e] **Georg von Hippel,**[a] **Harvey B. Meyer,**[a,b,c] **Kohtaroh Miura,**[a,b,c] **Konstantin Ottnad,**[a] **Andreas Risch**[f] **and Jonas Wilhelm**[a]

[a] *PRISMA$^+$ Cluster of Excellence and Institut für Kernphysik, Johannes Gutenberg-Universität Mainz, 55099 Mainz, Germany*

[b] *Helmholtz-Institut Mainz, Johannes Gutenberg-Universität Mainz, 55099 Mainz, Germany*

[c] *GSI Helmholtzzentrum für Schwerionenforschung, Planckstraße 1, 64291 Darmstadt, Germany*

[d] *Albert Einstein Center for Fundamental Physics (AEC) and Institut für Theoretische Physik, Universität Bern, Sidlerstrasse 5, 3012 Bern, Switzerland*

[e] *Aix-Marseille Université, Université de Toulon, CNRS, CPT, Marseille, France*

[f] *John von Neumann-Institut für Computing NIC, Deutsches Elektronen-Synchrotron DESY, Platanenallee 6, 15738 Zeuthen, Germany*

E-mail: msanjosp@uni-mainz.de,wittigh@uni-mainz.de

We present results for the hadronic running of the electromagnetic coupling and the weak mixing angle from simulations of lattice QCD with $N_f = 2{+}1$ flavours of $O(a)$-improved Wilson fermions. Using two different discretisations of the vector current, we compute the quark-connected and -disconnected contributions to the hadronic vacuum polarisation (HVP) functions $\bar{\Pi}^{\gamma\gamma}$ and $\bar{\Pi}^{Z\gamma}$ for spacelike squared momenta $Q^2 \leq 7$ GeV^2. Our results are extrapolated to the physical point using ensembles at four lattice spacings, with pion masses in the range from 130 to 420 MeV. We observe a tension of up to 3.5 standard deviations between our lattice results for $\Delta\alpha^{(5)}_{\rm had}(-Q^2)$ and estimates based on the R-ratio for space-like momenta in the range $Q^2 = 3 - 7\,\text{GeV}^2$. To obtain an estimate for $\Delta\alpha^{(5)}_{\rm had}(M_Z^2)$, we employ the Euclidean split technique. The implications for a comparison with global electroweak fits are assessed.

The 39th International Symposium on Lattice Field Theory, LATTICE2022
Rheinische Friedrich-Wilhelms-Universität Bonn
8th-13th August 2022

*Speaker

PoS(LATTICE2022)328

1. Introduction

Precision physics is one of the main avenues towards the discovery of particles and interactions beyond the Standard Model (BSM). In this approach, an improved experimental determination confronts an equally accurate theoretical prediction to disentangle well-known phenomena from small, novel effects. Electroweak global fits [1] are one particular consistency test where high precision is required. They constrain the Higgs boson mass from its loop contributions to well known quantities, such as the electromagnetic coupling at the Z-pole mass $\alpha(M_Z^2)$. The latter is usually predicted starting at the Thomson limit and studying the energy dependence, reaching the Z-pole eventually. As it turns out, the main source of uncertainty is the leading hadronic contribution at low energies, which is conventionally computed invoking the optical theorem and using experimentally measured $\sigma\left(e^+e^- \to \text{hadrons}\right)$ cross section-data [2–4]. Lattice determinations can replace the data-driven approach with an *ab initio* calculation, avoiding the complicated structure of resonances in the time-like region.

Another precision quantity is the weak mixing angle $\sin^2\theta_W$, whose value at low energies is sensitive to BSM physics but is strongly affected by hadronic uncertainties. In this regime it is accessible in neutrino-nucleus scattering experiments, atomic parity violation and parity-violating electron scattering, yet its value is known much less accurately than the fine-structure constant. The standard theoretical determination of its leading hadronic contribution employs the same electron-positron inelastic scattering data, but needs to separate the contribution from each quark flavour and re-weight it with the appropriate weak charge. Our alternative approach relying on lattice QCD allows for a better determination because it avoids the systematic uncertainty due to flavour separation.

Most of the work presented in this contribution has been published in Ref. [5], which can be consulted for further details and a complete set of references.

2. Lattice setup

Figure 1 shows the Coordinated Lattice Simulations (CLS) ensembles used in our analysis. They include $N_f = 2 + 1$ flavours of non-perturbatively $O(a)$-improved Wilson fermions, with a tree-level improved Lüscher-Weisz gauge action [6, 7]. Besides, we employ the *local* (L) and *point-split conserved* (C) discretisations for the quark-bilinears that we analyse in order to better constrain the continuum extrapolation, and all ensembles lie on the trajectory $m_\pi^2/2 + m_K^2 \approx \text{const}$. The quark loops for the quark-disconnected contribution constitute the most expensive part of the computation, and we calculate them using a variant of the method proposed in [8] combining the one-end trick [9] with the generalized hopping parameter expansion [10] and hierarchical probing [11]. The scale is set using $\sqrt{8t_0} = 0.415(4)(2)$ fm [7].

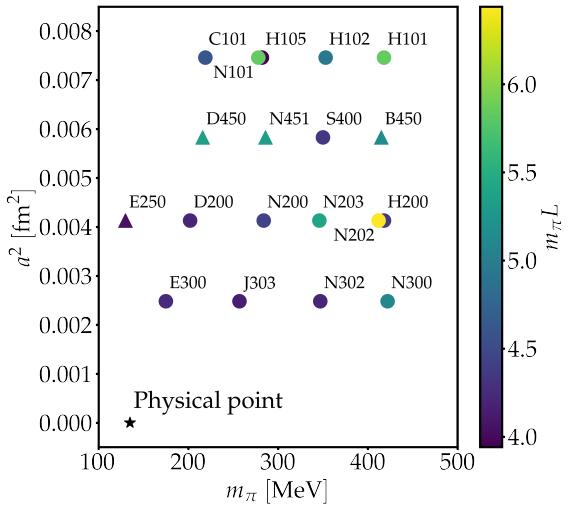

Figure 1: Landscape of CLS ensembles in terms of the lattice spacing a and pion mass m_π. Triangles (circles) indicate periodic (open) boundary conditions in time.

3. Time-momentum representation

The running electromagnetic coupling and weak mixing angle at momentum transfer q^2 are expressed as

$$\alpha(q^2) = \frac{\alpha(0)}{1-\Delta\alpha(q^2)}, \qquad \sin^2\theta_W(q^2) = \sin^2\theta_W(0)\left(1+\Delta\sin^2\theta_W(q^2)\right), \tag{1}$$

where $\alpha(0)$ and $\sin^2\theta_W(0)$ denote their values in the Thomson limit. The contributions to the running $\Delta\alpha(q^2)$ and $\Delta\sin^2\theta_W(q^2)$ are divided into leptonic and hadronic parts, where the former can be determined in perturbation theory, and we concentrate on the latter, which include non-perturbative phenomena at low momenta. At leading order in the electromagnetic coupling both quantities, $\Delta\alpha_{\text{had}}$ and $(\Delta\sin^2\theta_W)_{\text{had}}$, can be expressed in terms of the vacuum polarisation functions (VPFs) $\bar{\Pi}^{\gamma\gamma}$ and $\bar{\Pi}^{Z\gamma}$ according to

$$\Delta\alpha_{\text{had}}(q^2) = 4\pi\alpha(0)\bar{\Pi}^{\gamma\gamma}(q^2), \qquad (\Delta\sin^2\theta_W)_{\text{had}}(q^2) = -\frac{4\pi\alpha(0)}{\sin^2\theta_W(0)}\bar{\Pi}^{Z\gamma}(q^2), \tag{2}$$

where $\bar{\Pi}(q^2) = \Pi(q^2) - \Pi(0)$. The subtracted VPF $\bar{\Pi}^{\gamma\gamma}(q^2)$ describes all hadronic one-particle irreducible (1PI) diagrams one may introduce in a free photon propagator, while the corresponding quantity $\bar{\Pi}^{Z\gamma}(q^2)$ is relevant for the mixing between a photon and a Z boson. The VPFs $\bar{\Pi}^{\gamma\gamma}$ and $\bar{\Pi}^{Z\gamma}$ can be computed in lattice QCD for spacelike momentum transfers, $q^2 = -Q^2$, using the time-momentum representation (TMR) [12, 13]

$$\begin{aligned} \bar{\Pi}^{\alpha\gamma}(-Q^2) &= \int \mathrm{d}t\, G^{\alpha\gamma}(t)K(t,Q^2), \\ G^{\alpha\gamma}(t) &= -\frac{1}{3}\sum_{j=1,2,3}\int \mathrm{d}\vec{x}\,\left\langle V_j^\alpha(t,\vec{x})V_j^\gamma(0)\right\rangle_{\text{QCD}}, \quad \alpha = Z,\ \gamma, \end{aligned} \tag{3}$$

where V^γ is the electromagnetic current and V^Z is the vector component of the Z boson current. Since at $O(a)$ the breaking of global $\mathrm{SU}(N_f)$ symmetry by the quark mass matrix leads to a mixing between the local currents of different quark flavours, we decide to work in the isospin basis where renormalisation and $O(a)$ improvement are more easily implemented [14],

$$\begin{aligned} V^\gamma &= V^3 + 1/\sqrt{3}V^8 + 4/9V^c, \\ V^Z &= (1/2 - \sin^2\theta_W(0))V^\gamma - 1/6V^0 - 1/12V^c. \end{aligned} \tag{4}$$

Here, the isovector V^3, isoscalar V^8 and isosinglet V^0 components can be expressed in terms of the quark currents as

$$V^3 = \frac{1}{2}\left(V^u - V^d\right), \qquad V^8 = \frac{1}{2\sqrt{3}}\left(V^u + V^d - 2V^s\right), \qquad V^0 = \frac{1}{2}\left(V^u + V^d + V^s\right), \tag{5}$$

while V^c denotes the charm quark contribution. For the single-flavour quark-bilinears at the sink, we use either the L or C discretisations, while we always use the L case at the source. The kernel $K(t, Q^2) = t^2 - 4/Q^2 \sin^2(Qt/2)$ can, in principle, be evaluated at any Q^2. However, in practice we are limited by the lattice spacing and the box size, which are the cutoffs of our theory. In particular, choosing $Q^2 \sim (\pi/a)^2$ probes the correlator at short distances, where one finds strong discretisation effects. By contrast, $Q^2 \ll 1\,\mathrm{GeV}^2$ corresponds to the long-distance part of the correlator, which is noisier and suffers from stronger finite-size effects.

4. Analysis

To improve the signal-to-noise ratio for the vector correlators $G^{\gamma\gamma}(t)$ and $G^{Z\gamma}(t)$ at large times t, we apply the bounding method [15], using the effective mass for the correlator's lower bound, and the ground-state energy for the upper bound. For the isovector component, the latter corresponds to the ρ meson or the two-pion state, depending on the pion mass for a given ensemble. For the isoscalar, the ground level is either the three-pion state or the ω meson. It is also possible to bound $\bar{\Pi}^{08}$ using the effective mass as upper bound and the isoscalar ground state as lower bound [5, 16]. To obtain the correlators in infinite volume, we decompose the two-point functions in finite volume according to $G(t,\infty) = G(t,L) + \Delta G(t,L)$, where $G(t,L)$ is the correlator computed on the lattice in finite volume, and $\Delta G(t,L)$ denotes the correction for finite-size effects (FSE) on a given timeslice, which depend on the IR regulator L. To estimate $\Delta G(t,L)$, we have used the Meyer-Lellouch-Lüscher (MLL) method [17–19] and the Hansen-Patella (HP) procedure [20, 21]. Both methods produce consistent estimates for the finite-size correction, and we find that $\Delta G(t,L)$ amounts to a $\sim 2\%$ upward shift in the isovector component $\bar{\Pi}^{33}(-1\,\mathrm{GeV}^2)$ at $m_\pi L = 4$, while the effect is reduced to $\sim 0.2\%$ at $m_\pi L = 6$. In addition, we have two sets of ensembles with the same parameters but different volumes, as can be seen in Figure 1, and we observe good agreement between them once the FSE have been applied. Afterwards, we combine the extrapolation to the continuum $a \to 0$ and the interpolation to the isospin-symmetric pion $m_\pi^{\mathrm{phy}} = 134.9768(5)\,\mathrm{MeV}$ and kaon masses $m_K^{\mathrm{phy}} = 495.011(15)\,\mathrm{MeV}$ [1, 22]. To this end, we employ the dimensionless fit variables a^2/t_0^{sym}, $\phi_2 = 8t_0 m_\pi^2$, and $\phi_4 = 8t_0(m_\pi^2/2 + m_K^2)$, where t_0 is measured on each ensemble, and t_0^{sym} is taken at the symmetric point $m_\pi = m_K$ from [7]. Figure 2 shows the fit at $Q^2 = 1\,\mathrm{GeV}^2$.

For $\bar{\Pi}^{08}$, we only have CL-data, but one discretisation is sufficient as we do not discern any lattice spacing dependence. By performing the quark contractions, we infer that $\bar{\Pi}^{08} = 0$ whenever $m_\pi = m_K$, so our fit model must be proportional to the combination $\phi_4 - 3/2\phi_2$. In fact, a single parameter is enough to fit the data with $\chi^2/\text{dof} \sim 0.7$,

$$\bar{\Pi}^{08,\text{CL}}_{\text{model}} = \lambda_1 \left(\phi_4 - 3/2\phi_2\right). \tag{6}$$

For the $\bar{\Pi}^{cc}$ contribution, we decide to only use the CL-data, which have $O(10\%)$ discretisation effects, and drop the LL-data, for which these effects are as large as $O(40\%)$. Replacing t_0 by t_0^{sym} in the TMR kernel and the x-variable ϕ_2, the pion mass behaviour can be modelled using a linear term. This substitution introduces correlations among all ensembles at the same lattice spacing [7], which increases the size of the covariance matrix in our fit. Therefore, we decide to fit the charm contribution separately. Empirically, we find that an a^2-term is sufficient to describe lattice artefacts, and hence we fit the Ansatz

$$\bar{\Pi}^{cc}_{\text{con,model}} = \bar{\Pi}^{cc,\text{sym}}_{\text{con}} + \delta_2^{cc,\text{CL}} a^2/t_0^{\text{sym}} + \gamma_1^{cc}(\phi_2 - \phi_2^{\text{sym}}). \tag{7}$$

The subscript "con" indicates we only compute the quark-connected component. Fitting the entire set of ensembles, we obtain $\chi^2/\text{dof} \sim 3$, but this is probably a side-effect from the increased size of the covariance matrix. Removing the ensembles with $m_\pi > 400\,\text{MeV}$, we obtain $\chi^2/\text{dof} \sim 2$, and further removing ensembles with $m_\pi > 300\,\text{MeV}$ yields $\chi^2/\text{dof} \sim 0.8$. The cuts have a negligible effect on the expectation value, and the quality of the fit barely depends on Q^2 [16]. Moving on to the fit function for the CL isovector component $\bar{\Pi}^{33}$, we make the ansatz

$$\bar{\Pi}^{33,\text{CL}} = \bar{\Pi}^{\text{sym}} + \delta_2^{\text{C}} a^2/t_0^{\text{sym}} + \gamma_1^{33}\left(\phi_2 - \phi_2^{\text{sym}}\right) + \gamma_2^{33}\log\left(\phi_2/\phi_2^{\text{sym}}\right) + \eta_1(\phi_4 - \phi_4^{\text{sym}}). \tag{8}$$

The γ_1^{33} term models the dependence at large pion masses, while ChPT inspires the form of the γ_2^{33} term to model the singular behaviour towards $m_\pi \to 0$ [23]. Regarding the parameter η_1, we note that our ensembles fulfil $\phi_4 \approx \text{const}$, and the deviations from the exact equality can be modelled using a linear term. We also note that the fit parameters $\bar{\Pi}^{\text{sym}}$, ϕ_2^{sym} and $\phi_4^{\text{sym}} = 3/2\phi_2^{\text{sym}}$ determine the coordinates where $m_\pi = m_K$ and, since $\bar{\Pi}^{33} = \bar{\Pi}^{88}$ at this point, these set of parameters are common for both isospin channels. To model the CL isoscalar component, we use

$$\bar{\Pi}^{88,\text{CL}} = \bar{\Pi}^{\text{sym}} + \delta_2^{\text{CL}} a^2/t_0^{\text{sym}} + \gamma_1^{88}\left(\phi_2 - \phi_2^{\text{sym}}\right) + \gamma_2^{88}(\phi_2 - \phi_2^{\text{sym}})^2 + \eta_1(\phi_4 - \phi_4^{\text{sym}}). \tag{9}$$

Similar expressions are used for the LL-data. In this case, the model has a finite limit towards $m_\pi \to 0$, as expected in ChPT [23], although the particular form for both isospin channels is chosen such that the fit faithfully describes the result obtained on the ensemble at the physical pion mass (E250). Using eqs. (8) and (9), we obtain $\chi^2/\text{dof} \sim 1.5$ up to $Q^2 \gtrsim 2.5\,\text{GeV}^2$. Beyond this point, the increasing size of lattice artefacts requires the inclusion of an extra $(a^2/t_0^{\text{sym}})^{3/2}$ term in both eqs. (8) and (9), allowing us to reach $Q^2 \sim 7\,\text{GeV}^2$ with similar fit quality, albeit increasing the statistical error. We effect the transition between both models using a smooth step function centred around $2.5\,\text{GeV}^2$. At the physical point, with $Q^2 = 1\,\text{GeV}^2$, we obtain

$$\begin{aligned}\Delta\alpha_{\text{had}}(-1\,\text{GeV}^2)\times 10^6 &= 3864\ (17)\ (8)\ (22)\ (4)\ (12)\ [32,\ 0.8\,\%],\\ (\Delta\sin^2\theta_W)_{\text{had}}(-1\,\text{GeV}^2)\times 10^6 &= -3927\ (19)\ (5)\ (32)\ (4)\ (13)\ [40,\ 1.0\,\%],\end{aligned} \tag{10}$$

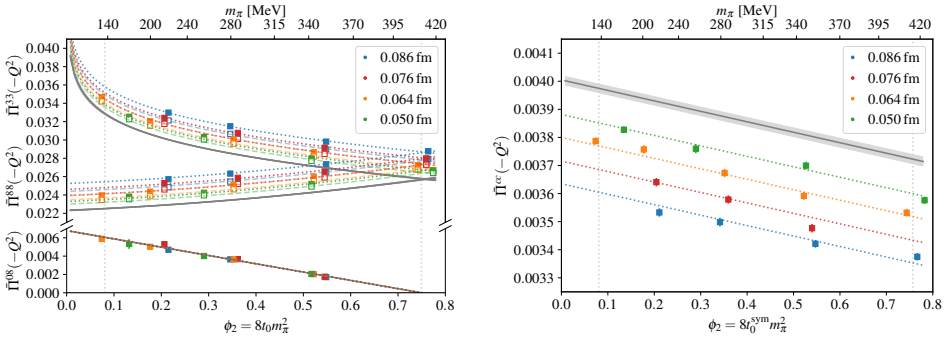

Figure 2: Extrapolation to the physical point at $Q^2 = 1\,\mathrm{GeV}^2$. Left: $\bar{\Pi}^{33}$, $\bar{\Pi}^{88}$ and $\bar{\Pi}^{08}$ contributions, incorporating the constraint $\bar{\Pi}^{33} = \bar{\Pi}^{88}$ at the SU(3)-symmetric point. Right: Extrapolation of the charm quark contribution $\bar{\Pi}^c$.

where the errors from left to right are from statistics, extrapolation, scale-setting, missing charm-quark loops and IB. In square brackets, we add all errors in quadrature. The last number on the right shows that we obtain a precision of $\sim 1\%$ at this particular momentum. The statistical error is propagated using bootstrap sampling, and the extrapolation uncertainty is obtained by repeating the fit removing the heavier pion masses. Note that the calibration of the lattice scale $\sqrt{8t_0} = 0.415\ (4)\ (2)$ fm [7] enters indirectly in our analysis ($\bar{\Pi}$ is dimensionless) through the TMR kernel and the definition of ϕ_2 and ϕ_4, and we estimate the final uncertainty propagating the error of t_0 using bootstrap sampling. We find ourselves in a favourable position, because $\sqrt{8t_0}$ is determined with 1% accuracy and it induces a $\sim 0.7\%$ error in the final quantities. Nonetheless, the scale-setting uncertainty is dominant in the range $0 < Q^2 \lesssim 3\,\mathrm{GeV}^2$. As a result, there is an ongoing effort to improve the determination of the scale, including IB effects [24]. Regarding the missing charm-quark contribution to the quark sea, we estimate the charm quenching effect phenomenologically, quantifying the contributions from D^+D^-, $D^0\bar{D}^0$ and $D_s^+D_s^-$ to the HVP treating the D-meson form factors in scalar QED. Besides, the valence charm-quark loops are negligible according to [15]. Finally, we have evaluated the quark-connected HVP in QCD + QED on one ensemble at $m_\pi \sim 220\,\mathrm{MeV}$. The result is used to estimate the relative size of the missing IB effects that we add to our error budget at the physical point. We repeat the extrapolation at several Q^2, distributed logarithmically, to probe the low-momentum region, and we plot the results in Figure 3. To provide the running in an analytic form, we use the fact that the HVP momentum dependence can be written as a Stieltjes function [25]. In turn, this can be approximated by a ratio of polynomials, i.e. a Padé approximant $R_M^N(Q^2)$, whose general expression is

$$R_M^N(Q^2) = \frac{\sum_{j=0}^{M} a_j Q^{2j}}{1 + \sum_{k=1}^{N} b_k Q^{2k}}. \tag{11}$$

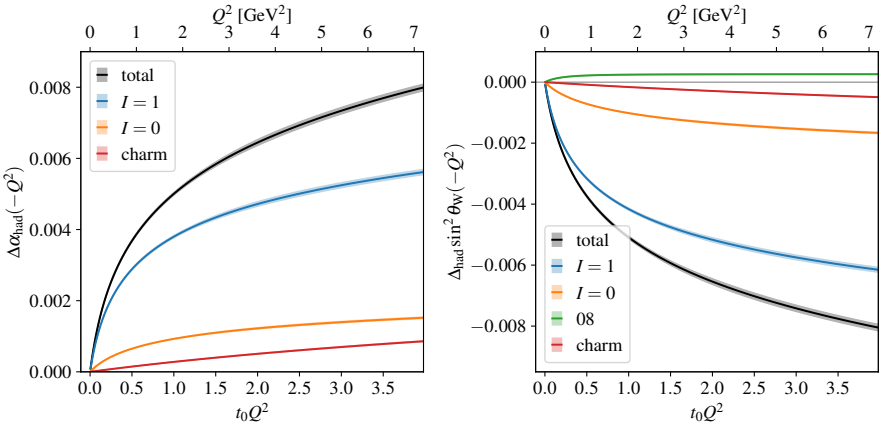

Figure 3: Leading hadronic contribution to the QED coupling and electroweak mixing angle, which appear in black. We also give the various components: charm G^{cc} in red, isoscalar G^{88} in orange, isovector G^{33} in blue, and mixing G^{08} in green. The band width indicates the total error.

Via a least-squares fit of $R_M^N(Q^2)$ to $\bar{\Pi}(-Q^2)$, we obtain

$$\begin{aligned}\Delta\alpha_{\rm had}(-Q^2) &= 4\pi\alpha\,\frac{0.1094(23)\,\mathrm{x}+0.093(15)\,\mathrm{x}^2+0.0039(6)\,\mathrm{x}^3}{1+2.85(22)\,\mathrm{x}+1.03(19)\,\mathrm{x}^2+0.0166(12)\,\mathrm{x}^3},\\ (\Delta\sin^2\theta_W)_{\rm had}(-Q^2) &= -\frac{4\pi\alpha}{\sin^2\theta_W}\,\frac{0.022\,63(6)\,\mathrm{x}+0.025(5)\,\mathrm{x}^2+0.000\,89(34)\,\mathrm{x}^3}{1+2.94(29)\,\mathrm{x}+1.12(27)\,\mathrm{x}^2+0.015(8)\,\mathrm{x}^3},\end{aligned} \tag{12}$$

with $\mathrm{x} = Q^2/\mathrm{GeV}^2$, $4\pi\alpha = 0.091\,701\,236\,853(14)$ and $\sin^2\theta_W = 0.238\,57(5)$ [1]. Note the parameter a_0 is zero since $\bar{\Pi}(0) = 0$. The choice $N = M = 3$ reproduces the data accurately, yet we observe that the extra fit parameters are poorly determined. In order to reproduce the error bands in Figure 3, we refer the reader to [5], where we also include the correlation matrix of the fit parameters.

5. The hadronic running of α at the Z-pole

The value of $\Delta\alpha^{(5)}_{\rm had}(q^2)$ at $q^2 = M_Z^2$ is a key quantity in electroweak precision physics. It serves, on the one hand, as an input quantity for the interpretation of experiments at high-energy colliders. On the other hand, direct theoretical determinations can be compared to the results of global electroweak fits, thereby providing a stringent test of the SM.

The traditional method to determine $\Delta\alpha^{(5)}_{\rm had}(M_Z^2)$ proceeds by evaluating a dispersion integral over the hadronic cross section ratio ("R-ratio") $R(s)$, according to

$$\Delta\alpha^{(5)}_{\rm had}(q^2) = -\frac{\alpha\,q^2}{3\pi}\,\fint_{m_{\pi_0}^2}^{\infty}\frac{R(s)}{s(s-q^2)}\,ds, \quad q^2 = M_Z^2, \quad R(s) = \frac{3s}{4\pi\alpha(s)}\,\sigma(e^+e^-\to\text{hadrons})\,. \tag{13}$$

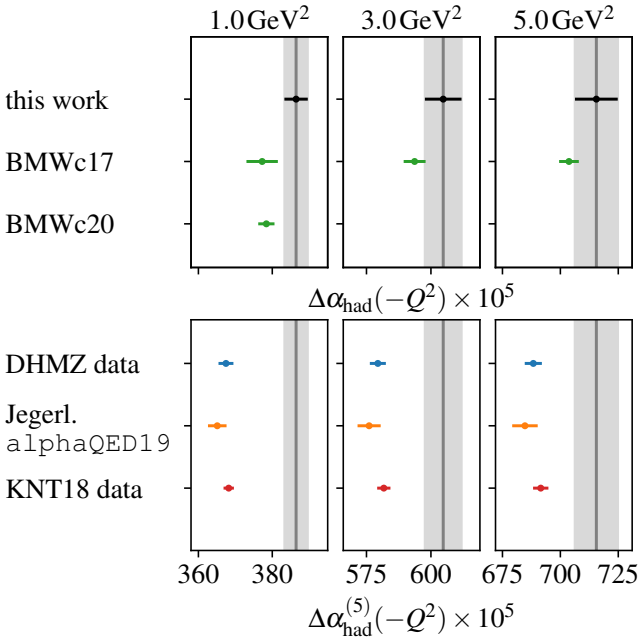

Figure 4: Comparison of the QED coupling at various momenta between our determination and several others. At the top half, the lattice determinations by BMWc [15, 26] and, at the bottom, the 5 flavours comparison with the phenomenological determinations by DHMZ [2], Jegerlehner [3], and KNT [4].

The above master formula is closely related to the corresponding dispersion integral for the leading-order hadronic vacuum polarisation contribution to the muon $g-2$, i.e.

$$a_\mu^{\rm LO,\,hvp} = \left(\frac{\alpha m_\mu}{3\pi}\right)^2 \int_{m_{\pi_0}^2}^{\infty} \frac{R(s)\,\hat{K}(s)}{s^2}\,ds, \quad 0.63 \le \hat{K}(s) \le 1\,. \tag{14}$$

This implies that the evaluation of $\Delta\alpha^{(5)}_{\rm had}(M_Z^2)$ by means of eq. (13) is affected by experimental uncertainties arising from experimentally measured hadronic cross sections in a similar manner than data-driven determinations of $a_\mu^{\rm LO,\,hvp}$.

An alternative approach to evaluate $\Delta\alpha^{(5)}_{\rm had}(M_Z^2)$ is based on the so-called Euclidean split technique (also dubbed the Adler function approach) [27–29], in which $\Delta\alpha^{(5)}_{\rm had}(M_Z^2)$ is divided into three separate contributions, according to

$$\Delta\alpha^{(5)}_{\rm had}(M_Z^2) = \Delta\alpha^{(5)}_{\rm had}(-Q_0^2) + \left[\Delta\alpha^{(5)}_{\rm had}(-M_Z^2) - \Delta\alpha^{(5)}_{\rm had}(-Q_0^2)\right] + \left[\Delta\alpha^{(5)}_{\rm had}(M_Z^2) - \Delta\alpha^{(5)}_{\rm had}(-M_Z^2)\right]. \tag{15}$$

It is primarily the first term on the right-hand side, $\Delta\alpha^{(5)}_{\rm had}(-Q_0^2)$, that absorbs the bulk of the non-perturbative physics, depending on the choice of the Euclidean squared momentum transfer Q_0^2. In particular, the first term in square brackets on the RHS of eq. (15) can be computed as an integral over the Adler function $D(Q^2)$, defined by

$$D(-s) := \frac{3\pi}{\alpha}\, s\, \frac{d}{ds}\Delta\alpha_{\rm had}(s)\,, \tag{16}$$

and which is known in massive QCD perturbation theory at three loops [27, 29, 30]. Integrating eq. (16) for spacelike momentum transfers from Q_0^2 to M_Z^2 yields

$$\left[\Delta\alpha^{(5)}_{\rm had}(-M_Z^2) - \Delta\alpha^{(5)}_{\rm had}(-Q_0^2)\right]_{\rm pQCD/Adler} = \frac{\alpha}{3\pi}\int_{Q_0^2}^{M_Z^2}\frac{dQ^2}{Q^2}\,D(Q^2). \tag{17}$$

Furthermore, by inserting the dispersion integral for $\Delta\alpha_{\rm had}$ into eq. (16) one obtains a representation of $D(Q^2)$ in terms of the R-ratio, i.e.

$$D(Q^2) = Q^2\int_{m_{\pi_0^2}}^{\infty}\frac{R(s)}{(s+Q^2)^2}\,ds\,, \tag{18}$$

and a straightforward calculation shows that the second term on the RHS of eq. (15) can also be expressed as

$$\left[\Delta\alpha^{(5)}_{\rm had}(-M_Z^2) - \Delta\alpha^{(5)}_{\rm had}(-Q_0^2)\right]_{\rm disp.} = \frac{\alpha(M_Z^2-Q_0^2)}{3\pi}\int_{m_{\pi_0^2}}^{\infty}\frac{R(s)}{(s+Q_0^2)(s+M_Z^2)}ds\,. \tag{19}$$

The freedom to evaluate this quantity either in perturbative QCD or in terms of the experimentally mesured R-ratio allows for a valuable cross check. Finally, the third term on the RHS of eq. (15) provides the link between spacelike and timelike regimes, which, at energies as large as the Z boson mass, can be reliably determined in perturbation theory [3, 31], viz.

$$\left[\Delta\alpha^{(5)}_{\rm had}(M_Z^2) - \Delta\alpha^{(5)}_{\rm had}(-M_Z^2)\right] = 0.000\,045(2)\,. \tag{20}$$

The Euclidean split technique holds several advantages over the standard method based on dispersion integrals:

- The integration in eq. (17) is performed over Euclidean squared momenta, and therefore the integration over resonances and physical thresholds, which renders the evaluation of the dispersion integrals in eqs. (13) and (14) quite intricate, can be avoided.
- The non-perturbative threshold value $\Delta\alpha^{(5)}_{\rm had}(-Q_0^2)$ can be determined either via dispersion theory and the experimental R-ratio or in lattice QCD. In the future, there is also the possibility of a direct experimental measurement from the MUonE experiment [32, 33]. By contrast, the direct evaluation of $\Delta\alpha^{(5)}_{\rm had}(M_Z^2)$ via dispersion integrals requires precise experimental data up to much higher energies compared to $\Delta\alpha^{(5)}_{\rm had}(-Q_0^2)$.

6. Estimate of $\Delta\alpha^{(5)}_{\rm had}(M_Z^2)$ from lattice QCD

In order to produce an estimate for $\Delta\alpha^{(5)}_{\rm had}(M_Z^2)$, we substitute our lattice results obtained at small Euclidean momentum transfers for the offset value $\Delta\alpha^{(5)}_{\rm had}(-Q_0^2)$ in eq. (15). Furthermore, we employ the Adler function to determine the running from low to high Euclidean momenta, by computing $[\Delta\alpha^{(5)}_{\rm had}(-M_Z^2) - \Delta\alpha^{(5)}_{\rm had}(-Q_0^2)]_{\rm pQCD/Adler}$ using the software package `pQCD/Adler` by Jegerlehner [36]. In order to assess the uncertainty due to the ambiguity in the choice of the threshold scale Q_0^2, we plot in Fig. 5 the resulting estimates for $\Delta\alpha^{(5)}_{\rm had}(M_Z^2)$ as a function of Q_0^2.

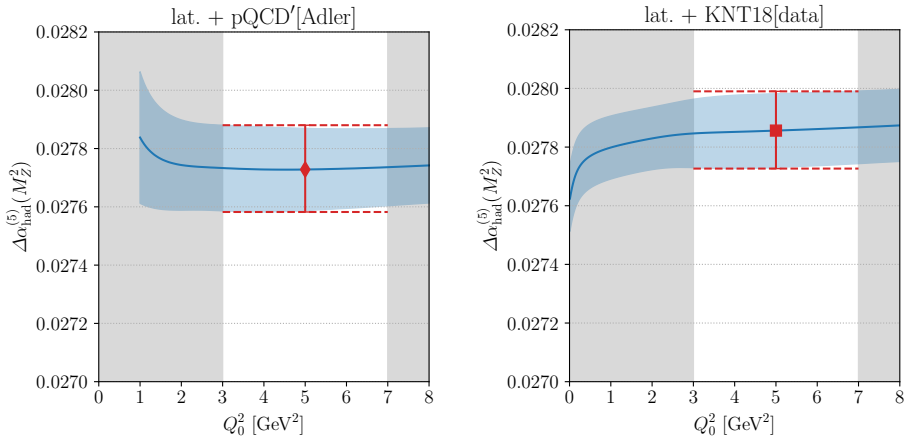

Figure 5: Left: The hadronic running of α at the Z pole, evaluated via the Euclidean split techniques and eq. (17), plotted as a function of the threshold scale, Q_0^2. Right: the same quantity with the running evaluated via dispersion theory accoring to eq. (19), using the R-ratio data and covariance matrix from [34, 35]. The red point in both panels represents the final estimate, while the horizontal dashed lines denote the uncertainty due to the choice of Q_0^2 as inferred from the maximum and minimum values within the interval from 3 to 7 GeV^2.

We observe stability in the estimates for $\Delta\alpha^{(5)}_{\rm had}(M_Z^2)$ when Q_0^2 is varied between 3 and 7 GeV^2. As a cross check, we have determined the running using dispersion theory (see eq. (19)), and the resulting estimates for $\Delta\alpha^{(5)}_{\rm had}(M_Z^2)$ are again plotted versus Q_0^2 in the right panel of Fig. 5. We find that both alternatives yield very compatible results within errors. As our final estimate we quote the result based on the integration of the perturbative Adler function, i.e.

$$\Delta\alpha^{(5)}_{\rm had}(M_Z^2) = 0.027\,73(9)_{\rm lat}(2)_{\rm btm}(12)_{\rm pQCD}\,[15]_{\rm tot}\,, \tag{21}$$

where the first error is the intrinsic error of our lattice calculation, including the ambiguity in the choice of Q_0^2, the second is an estimate of the uncertainty due to the missing bottom quark contribution, and the last error arises from the running from Q_0^2 to M_Z^2 is evaluated in terms of the integrated Adler function computed in perturbative QCD. The final number in square brackets denotes the total error after summing the individual uncertainties in quadrature.

It is instructive to study the relative size of the individual contributions in the Euclidean split technique, eq. (15), as a function of Q_0^2. This is illustrated by the pie charts in Fig. 6, where the top row shows the relative size of the individual terms that make up the central value of $\Delta\alpha^{(5)}_{\rm had}(M_Z^2)$, while the charts in the bottom row represent their contributions to the variance. This exercise shows that the scale Q_0^2 can be used to optimise the reliability and precision of $\Delta\alpha^{(5)}_{\rm had}(M_Z^2)$. For instance, a significant reduction of the total error in the lattice calculation will do little to improve the overall precision of $\Delta\alpha^{(5)}_{\rm had}(M_Z^2)$ if the threshold scale is fixed at 3 GeV^2. From the charts in the figure one reads off that our lattice calculation accounts for $\sim 25\%$ of the value of the hadronic running and for $(25-50)\%$ of the variance, depending on the value of Q_0^2 in the interval between 3 and 7 GeV^2.

In Fig. 7 we compare our results with other direct estimates obtained via the data-driven approach and the results from global electroweak fits. Our preferred result of eq. (21) is shown as the grey vertical band. Within the quoted errors, it agrees very well with the determinations based on

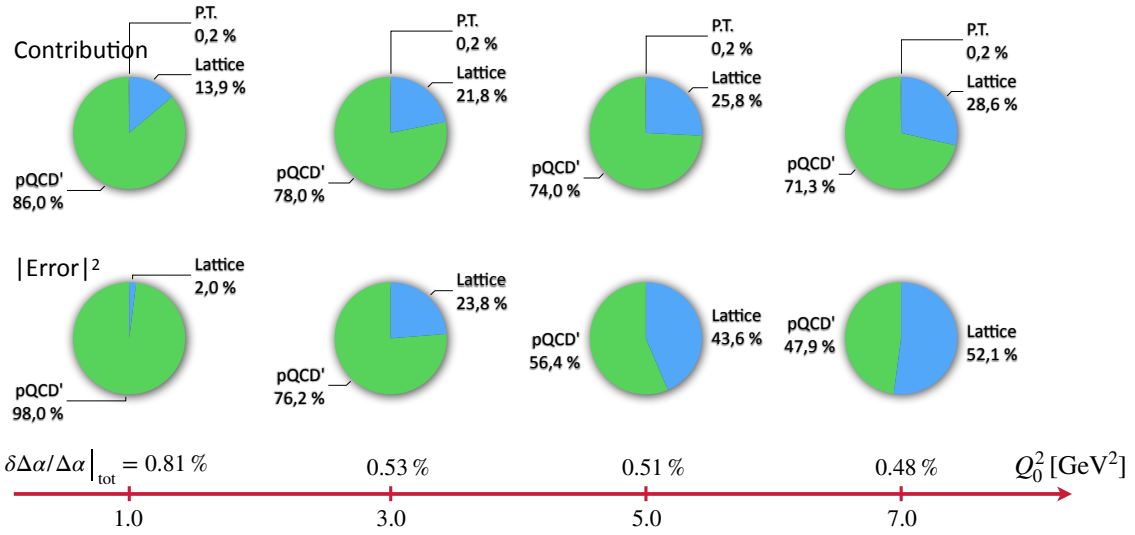

Figure 6: Pie charts showing the relative contribution to $\Delta\alpha^{(5)}_{\rm had}(M_Z^2)$ from the Euclidean split technique, for several values of Q_0^2. The running between Q_0^2 and M_Z^2 is evaluated using the perturbative Adler function. The top and bottom rows show the contributions to the value and the variance, respectively.

the R-ratio shown as green points in the middle panel. For instance, Jegerlehner [3] quotes a value of $\Delta\alpha^{(5)}_{\rm had}(M_Z^2) = 0.027\,52(12)$ using the R-ratio for fixing the non-perturbative input at $Q_0^2 = 4\,\text{GeV}^2$ and the perturbative Adler function for the running. At first sight, the agreement between the vertical grey band and the green points in the middle panel of Fig. 7 appears to contradict our earlier observation of a tension between lattice and data-driven evaluations of $\Delta\alpha_{\rm had}(-Q_0^2)$ for $Q_0^2 \lesssim 7\text{GeV}^2$ (see Fig. 4). The resolution of what seems like a contradiction comes from the observation that the running from low to high Euclidean momenta is correlated between the two approaches. In other words, both lattice and data-driven determinations of $\Delta\alpha^{(5)}_{\rm had}(M_Z^2)$ share the correlated uncertainty in the evaluation of $[\Delta\alpha^{(5)}_{\rm had}(-M_Z^2) - \Delta\alpha^{(5)}_{\rm had}(-Q_0^2)]$, which must be dropped when computing the difference between the two methods.

In the bottom panel of Fig. 7 we plot various results from global electroweak fits. Although the latter mostly favour slightly smaller values for the hadronic running, the results are not in contradiction with our lattice estimate, given the relatively large errors.

7. Conclusions

We have presented results for the leading hadronic contribution to the running of the electromagnetic coupling $\Delta\alpha_{\rm had}(-Q^2)$ and the electroweak mixing angle $(\Delta\sin^2\theta_W)_{\rm had}(-Q^2)$ in the range of space-like momenta $Q^2 \leq 7\,\text{GeV}^2$. We have estimated all sources of uncertainty and find that the scale-setting error dominates for $Q^2 \leq 3\,\text{GeV}^2$. For larger momenta, it is necessary to include an extra a^3 term in the continuum extrapolation, which increases the statistical error. Overall, we achieve 1% precision for both quantities in the region $Q^2 > 1\,\text{GeV}^2$, and 2% for smaller momenta. Our main results are provided in the form of analytic functions for $\Delta\alpha_{\rm had}(-Q^2)$ and $(\Delta\sin^2\theta_W)_{\rm had}(-Q^2)$, given in eq. (12) in terms of Padé Ansätze. Together with the corresponding correlation matrices for the parameters a_j, b_k [5], it is possible to reproduce our results and total

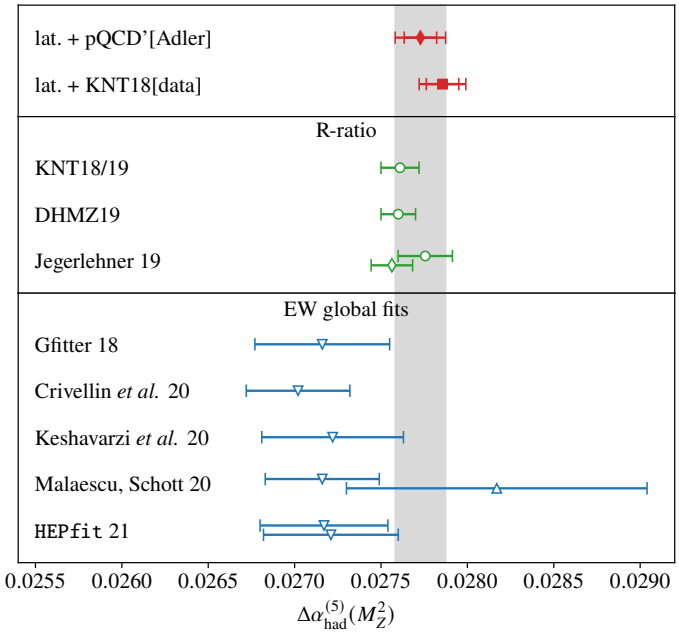

Figure 7: Compilation of results for $\Delta\alpha^{(5)}_{\rm had}(M_Z^2)$. Our lattice estimates are shown as red symbols, with our preferred result, listed in eq. (21) shown as the grey vertical band. Green circles represent results based on dispersion theory [2–4, 34], where the R-ratio integration is performed over the entire momentum range. Jegerlehner's estimate applying the Euclidean split technique with dispersive input for $\Delta\alpha_{\rm had}(-Q_0^2)$ is shown as the green open diamond. Open blue downward pointing triangles show results from global electroweak fits [37–41] with $\Delta\alpha_{\rm had}(M_Z^2)$ as a free fit parameter. The upward pointing open triangle denotes a fit in which the Higgs mass is left as another free parameter.

uncertainty at any small space-like momentum Q^2. Our result for $\Delta\alpha$ compares well with the lattice determinations by the BMW collaboration [15, 26], with only a mild tension of 1 σ to 2 σ. However, we observe a significant discrepancy of more than 3σ with the phenomenological determinations by DHMZ [2], Jegerlehner [3], and KNT [4].

Given the close relation between the hadronic running of α and the hadronic vacuum polarisation contribution to the muon $g-2$, the observation of a tension in $\Delta\alpha$ between lattice and data-driven estimates is consistent with the apparent discrepancy for the intermediate window observable derived from $a_\mu^{\rm LO,\,hvp}$ [26, 42, 43]. In spite of the observed tension with data-driven approaches, we find that the conversion of our lattice result for $\Delta\alpha_{\rm had}(-Q_0^2)$ into an estimate for $\Delta\alpha^{(5)}_{\rm had}(M_Z^2)$ broadly agrees with global electroweak fits. Our calculation, therefore, is not in contradiction with the SM, and we conclude that the SM can accommodate a larger value for a_μ without producing a significant tension with electroweak data, at least at the current level of precision.

Acknowledgements

Calculations for this project have been performed on the HPC clusters Clover and HIMster-II at Helmholtz Institute Mainz and on Mogon-II at Johannes Gutenberg-Universität (JGU) Mainz, on the HPC systems JUQUEEN and JUWELS at Jülich Supercomputing Centre (JSC), and on Hazel

Hen at Höchstleistungsrechenzentrum Stuttgart (HLRS). The authors gratefully acknowledge the support of the Gauss Centre for Supercomputing (GCS) and the John von Neumann-Institut für Computing (NIC) for project HMZ21 and HMZ23 at JSC and project GCS-HQCD at HLRS. We are grateful to our colleagues in the CLS initiative for sharing ensembles. This work has been supported by Deutsche Forschungsgemeinschaft (German Research Foundation, DFG) through project HI 2048/1-2 (project No. 399400745) and through the Cluster of Excellence "Precision Physics, Fundamental Interactions and Structure of Matter" (PRISMA+ EXC 2118/1), funded within the German Excellence strategy (Project ID 39083149). A.G. received funding from the Excellence Initiative of Aix-Marseille University - A*MIDEX, a French "Investissements d'Avenir" programme, AMX-18-ACE-005 and from the French National Research Agency under the contract ANR-20-CE31-0016.

References

[1] Particle Data Group collaboration, *Review of Particle Physics*, *PTEP* **2020** (2020) 083C01.

[2] M. Davier, A. Hoecker, B. Malaescu and Z. Zhang, *A new evaluation of the hadronic vacuum polarisation contributions to the muon anomalous magnetic moment and to* $\alpha(m_Z^2)$, *Eur. Phys. J. C* **80** (2020) 241 [1908.00921].

[3] F. Jegerlehner, $\alpha_{\rm QED,eff}(s)$ *for precision physics at the FCC-ee/ILC*, *CERN Yellow Reports: Monographs* **3** (2020) 9.

[4] A. Keshavarzi, D. Nomura and T. Teubner, $g-2$ *of charged leptons,* $\alpha(M_Z^2)$ *, and the hyperfine splitting of muonium*, *Phys. Rev. D* **101** (2020) 014029 [1911.00367].

[5] M. Cè, A. Gérardin, G. von Hippel, H.B. Meyer, K. Miura, K. Ottnad et al., *The hadronic running of the electromagnetic coupling and the electroweak mixing angle from lattice QCD*, *JHEP* **08** (2022) 220 [2203.08676].

[6] M. Bruno et al., *Simulation of QCD with* $N_f = 2 + 1$ *flavors of non-perturbatively improved Wilson fermions*, *JHEP* **02** (2015) 043 [1411.3982].

[7] M. Bruno, T. Korzec and S. Schaefer, *Setting the scale for the CLS* $2+1$ *flavor ensembles*, *Phys. Rev. D* **95** (2017) 074504 [1608.08900].

[8] L. Giusti, T. Harris, A. Nada and S. Schaefer, *Frequency-splitting estimators of single-propagator traces*, *Eur. Phys. J. C* **79** (2019) 586 [1903.10447].

[9] C. McNeile and C. Michael, *Decay width of light quark hybrid meson from the lattice*, *Phys. Rev. D* **73** (2006) 074506 [hep-lat/0603007].

[10] V. Gülpers, G. von Hippel and H. Wittig, *Scalar pion form factor in two-flavor lattice QCD*, *Phys. Rev. D* **89** (2014) 094503 [1309.2104].

[11] A. Stathopoulos, J. Laeuchli and K. Orginos, *Hierarchical probing for estimating the trace of the matrix inverse on toroidal lattices*, 1302.4018.

[12] D. Bernecker and H.B. Meyer, *Vector correlators in lattice QCD: Methods and applications*, *European Physical Journal A* **47** (2011) 148 [1107.4388].

[13] A. Francis, B. Jäger, H.B. Meyer and H. Wittig, *New representation of the Adler function for lattice QCD*, *prd* **88** (2013) 054502 [1306.2532].

[14] A. Gérardin, T. Harris and H.B. Meyer, *Nonperturbative renormalization and $O(a)$-improvement of the nonsinglet vector current with $N_f = 2+1$ Wilson fermions and tree-level Symanzik improved gauge action*, *Phys. Rev. D* **99** (2019) 014519 [1811.08209].

[15] S. Borsányi et al., *Hadronic vacuum polarization contribution to the anomalous magnetic moments of leptons from first principles*, *Phys. Rev. Lett.* **121** (2018) 022002 [1711.04980].

[16] M.T. San José Pérez, *The hadronic contribution to the running of the electromagnetic coupling and the electroweak mixing angle*, Ph.D. thesis, Mainz, 2022. http://doi.org/10.25358/openscience-7115.

[17] H. Meyer, *Lattice QCD and the Timelike Pion Form Factor*, *Phys. Rev. Lett.* **107** (2011) 072002 [1105.1892].

[18] L. Lellouch and M. Lüscher, *Weak transition matrix elements from finite volume correlation functions*, *Commun. Math. Phys.* **219** (2001) 31 [hep-lat/0003023].

[19] M. Lüscher, *Signatures of unstable particles in finite volume*, *Nucl. Phys. B* **364** (1991) 237.

[20] M.T. Hansen and A. Patella, *Finite-volume effects in $(g-2)_\mu^{HVP,LO}$*, *Phys. Rev. Lett.* **123** (2019) 172001 [1904.10010].

[21] M.T. Hansen and A. Patella, *Finite-volume and thermal effects in the leading-HVP contribution to muonic $(g-2)$*, *JHEP* **10** (2020) 029 [2004.03935].

[22] A. Risch and H. Wittig, *Leading isospin breaking effects in the HVP contribution to a_μ and to the running of α*, *PoS* **LATTICE2021** (2022) 106 [2112.00878].

[23] M. Golterman, K. Maltman and S. Peris, *Chiral extrapolation of the leading hadronic contribution to the muon anomalous magnetic moment*, *Phys. Rev. D* **95** (2017) 074509 [1701.08685].

[24] A.M. Segner, A.D. Hanlon, R.J. Hudspith, A. Risch and H. Wittig, *Isospin-breaking Effects in Octet and Decuplet Baryon Masses*, *PoS* **LATTICE2021** (2022) 095 [2112.08262].

[25] C. Aubin, T. Blum, M. Golterman and S. Peris, *Model-independent parametrization of the hadronic vacuum polarization and g-2 for the muon on the lattice*, *Phys. Rev. D* **86** (2012) 054509 [1205.3695].

[26] S. Borsányi et al., *Leading hadronic contribution to the muon magnetic moment from lattice QCD*, *Nature* **593** (2021) 51 [2002.12347].

[27] S. Eidelman, F. Jegerlehner, A.L. Kataev and O. Veretin, *Testing nonperturbative strong interaction effects via the Adler function*, *Phys. Lett. B* **454** (1999) 369 [hep-ph/9812521].

[28] F. Jegerlehner, *Hadronic effects in $(g-2)_\mu$ and $\alpha_{\rm QED}(M_Z)$: Status and perspectives*, in *4th International Symposium on Radiative Corrections: Applications of Quantum Field Theory to Phenomenology*, pp. 75–89, 1, 1999 [hep-ph/9901386].

[29] F. Jegerlehner, *The running fine structure constant $\alpha(E)$ via the Adler function*, *Nucl. Phys. B Proc. Suppl.* **181-182** (2008) 135 [0807.4206].

[30] K.G. Chetyrkin, J.H. Kühn and M. Steinhauser, *Three-loop polarization function and $O(\alpha_s^2)$ corrections to the production of heavy quarks*, *Nucl. Phys. B* **482** (1996) 213 [hep-ph/9606230].

[31] F. Jegerlehner, *Hadronic Contributions to Electroweak Parameter Shifts: A Detailed Analysis*, *Z. Phys. C* **32** (1986) 195.

[32] G. Venanzoni, *The MUonE experiment: a novel way to measure the leading order hadronic contribution to the muon g-2*, *PoS* **ICHEP2018** (2019) 519 [1811.11466].

[33] A. Masiero, P. Paradisi and M. Passera, *New physics at the MUonE experiment at CERN*, *Phys. Rev. D* **102** (2020) 075013 [2002.05418].

[34] A. Keshavarzi, D. Nomura and T. Teubner, *Muon $g-2$ and $\alpha(M_Z^2)$: a new data-based analysis*, *Phys. Rev. D* **97** (2018) 114025 [1802.02995].

[35] A. Keshavarzi, D. Nomura and T. Teubner, "Space-like $\Delta\alpha^{(5)}_{\rm had}(-Q^2)$ data, including correlations." private communication.

[36] F. Jegerlehner, `pQCDAdler`, 2012. http://www-com.physik.hu-berlin.de/~fjeger/software.html.

[37] J. Haller, A. Hoecker, R. Kogler, K. Mönig, T. Peiffer and J. Stelzer, *Update of the global electroweak fit and constraints on two-Higgs-doublet models*, *Eur. Phys. J. C* **78** (2018) 675 [1803.01853].

[38] A. Crivellin, M. Hoferichter, C.A. Manzari and M. Montull, *Hadronic vacuum polarization: $(g-2)_\mu$ versus global electroweak fits*, *Phys. Rev. Lett.* **125** (2020) 091801 [2003.04886].

[39] A. Keshavarzi, W.J. Marciano, M. Passera and A. Sirlin, *Muon $g-2$ and $\Delta\alpha$ connection*, *Phys. Rev. D* **102** (2020) 033002 [2006.12666].

[40] B. Malaescu and M. Schott, *Impact of correlations between a_μ and $\alpha_{\rm QED}$ on the EW fit*, *Eur. Phys. J. C* **81** (2021) 46 [2008.08107].

[41] J. de Blas, M. Ciuchini, E. Franco, A. Goncalves, S. Mishima, M. Pierini et al., *Global analysis of electroweak data in the Standard Model*, *Phys. Rev. D* **106** (2022) 033003 [2112.07274].

[42] M. Cè et al., *Window observable for the hadronic vacuum polarization contribution to the muon* $g-2$ *from lattice QCD*, 2206.06582.

[43] C. Alexandrou et al., *Lattice calculation of the short and intermediate time-distance hadronic vacuum polarization contributions to the muon magnetic moment using twisted-mass fermions*, 2206.15084.